[CANCER RESEARCH 63, 2409–2415, May 15, 2003]

Metabolic Activation of Temozolomide Measured *in Vivo* Using Positron Emission Tomography[1]

Azeem Saleem, Gavin D. Brown, Frank Brady, Eric O. Aboagye, Safiye Osman, Sajinder K. Luthra, Alex S. O. Ranicar, Cathryn S. Brock, Malcolm F. G. Stevens, Edward Newlands, Terry Jones, and Pat Price[2]

Cancer Research United Kingdom Positron Emission Tomography Oncology Group, Imperial College London [A. S., G. D. B., E. O. A., C. S. B., P. P.] and Imaging Research Solutions Ltd. [F. B., S. O., S. K. L., A. S. O. R.], Hammersmith Hospital, London W12 0NN, United Kingdom; Medical Research Council Cyclotron Unit, Imperial College London, Cyclotron Building, Hammersmith Hospital, Du Cane Road, London W12 0HS, United Kingdom [T. J.]; Cancer Research Laboratories, School of Pharmaceutical Sciences, University of Nottingham, Nottingham NG7 2RD, United Kingdom [M. F. G. S.]; and Department of Medical Oncology, Charing Cross Hospital, Fulham Palace Road, London W6 8RF, United Kingdom [E. N.]

ABSTRACT

The purpose of this research was to quantitate and confirm the mechanism of *in vivo* metabolic activation of temozolomide. The secondary aims were to evaluate the tumor, normal tissue, and plasma pharmacokinetics of temozolomide *in vivo,* and to determine whether such pharmacokinetics resulted in tumor targeting.

[^{11}C]temozolomide kinetics were studied in men using positron emission tomography (PET). It has been postulated that temozolomide undergoes decarboxylation and ring opening in the 3–4 position to produce the highly reactive methyldiazonium ion that alkylates DNA. To investigate this, a dual radiolabeling strategy, with [^{11}C]temozolomide separately radiolabelled in the 3-*N*-methyl and 4-carbonyl positions, was used. We hypothesized that ^{11}C in the C-4 position of [4-^{11}C-carbonyl]temozolomide would be converted to [^{11}C]CO_2 if the postulated mechanism of metabolic conversion was true resulting in lower [^{11}C]temozolomide tumor exposure. Paired studies were performed with both forms of [^{11}C]temozolomide in 6 patients with gliomas. Another PET scan with ^{11}C-radiolabelled bicarbonate was performed and used to account for the metabolites of temozolomide using a data-led analytical approach. Plasma was analyzed for [^{11}C]temozolomide and [^{11}C]metabolites throughout the scan duration. Exhaled air was also sampled throughout the scan for [^{11}C]CO_2. The percentage ring opening of temozolomide over 90 min was also calculated to evaluate whether there was a differential in metabolic breakdown among plasma, normal tissue, and tumor.

There was rapid systemic clearance of both radiolabelled forms of [^{11}C]temozolomide over 90 min (0.2 liter/min/m^2), with [^{11}C]CO_2 being the primary elimination product. Plasma [^{11}C]CO_2 was present in all of the studies with [4-^{11}C-carbonyl]temozolomide and in half the studies with [3-*N*-^{11}C-methyl]temozolomide. The mean contributions to total plasma activity by [^{11}C]CO_2 at 10 and 90 min were 12% and 28% with [4-^{11}C-carbonyl]temozolomide, and 1% and 4% with [3-*N*-^{11}C-methyl]temozolomide, respectively. There was a 5-fold increase in exhaled [^{11}C]CO_2 sampled with [4-^{11}C-carbonyl]temozolomide compared with [3-*N*-^{11}C-methyl]temozolomide ($P < 0.05$). A decrease in tissue exposure [area under the curve between 0 and 90 min ($AUC_{0-90\ min}$)] to [^{11}C]temozolomide was also observed with [4-^{11}C-carbonyl] temozolomide compared with [3-*N*-^{11}C-methyl]temozolomide. Of potential therapeutic advantage was the higher [^{11}C]radiotracer and [^{11}C]temozolomide exposure ($AUC_{0-90\ min}$) in tumors compared with normal tissue. [^{11}C]temozolomide ring opening over 90 min was less in plasma (20.9%; $P < 0.05$) compared with tumor (26.8%), gray matter (29.7%), and white matter (30.1%), with no differences ($P > 0.05$) between tumor and normal tissues.

The significantly higher amounts of [^{11}C]CO_2 sampled in plasma and exhaled air, in addition to the lower normal tissue and tumor [^{11}C]temozolomide $AUC_{0-90\ min}$ observed with [4-^{11}C-carbonyl]temozolomide, confirmed the postulated mechanism of metabolic activation of temozolomide. A higher tumor [^{11}C]temozolomide $AUC_{0-90\ min}$ in tumors compared with normal tissue and the tissue-directed metabolic activation of temozolomide may confer potential therapeutic advantage in the activity of this agent. This is the first report of a clinical PET study used to quantify and confirm the *in vivo* mechanism of metabolic activation of a drug.

INTRODUCTION

Temozolomide is an alkylating agent of the imidazo[5,1-d]-1,2,3,5-tetrazine series (1). It has good oral bioavailability (2, 3), and has shown significant clinical activity against malignant melanomas and gliomas (4). Temozolomide is structurally related to the antimelanoma drug DTIC;[3] both agents require conversion to MTIC for their clinical activity. Whereas DTIC is metabolically activated to MTIC in the liver, the conversion of temozolomide to MTIC is postulated to be pH dependent (5). It has been proposed that temozolomide undergoes decarboxylation and ring opening to form MTIC, which is additionally fragmented to produce the highly reactive methyldiazonium ion that alkylates DNA (Fig. 1). Temozolomide is robustly stable under acid conditions, but the rate of degradation increases rapidly on passing through neutral to basic pH (6). This pH-dependent activation of temozolomide may provide an important basis of targeted therapy directed toward tumors (such as gliomas), which are known to have a higher pH compared with surrounding brain tissue.

PET is a highly sensitive and quantitative imaging technique by which *in vivo* drug pharmacokinetics can be assessed using tracer quantities of the drug labeled with positron-emitting radioisotopes (7, 8). In this study we have used PET to investigate the *in vivo* mechanism of action of temozolomide in men including investigation of any differential in chemical conversion of temozolomide in tumor compared with plasma and normal tissue. PET studies were conducted in patients with gliomas with ^{11}C-radiolabeled temozolomide using a dual labeling strategy. Paired PET studies were performed after injection of [^{11}C]temozolomide radiolabeled in two different positions *i.e.* at 4-carbonyl and 3-*N*-methyl positions of the molecule. We hypothesized that if the proposed mechanism of action was true, then ring opening of [^{11}C]temozolomide at the 3–4 position would lead to the formation of [^{11}C]CO_2 with [4-^{11}C-carbonyl]temozolomide, whereas with [3-*N*-^{11}C-methyl]temozolomide the label will ultimately be incorporated into DNA (Fig. 1). The [^{11}C]CO_2 produced during the metabolism of [^{11}C]temozolomide was quantified in plasma and exhaled air. Because PET is unable to distinguish radiolabeled chemical species *in vivo*, the contribution of [^{11}C]CO_2 to the tissue image was elucidated using spectral analysis, a data-led analytical method. This required an additional PET study after the injection of ^{11}C-labeled bicarbonate (which rapidly equilibrates with [^{11}C]CO_2 in blood aided by carbonic anhydrase in the body) to derive a relationship between

Received 9/25/02; accepted 3/14/03.

The costs of publication of this article were defrayed in part by the payment of page charges. This article must therefore be hereby marked *advertisement* in accordance with 18 U.S.C. Section 1734 solely to indicate this fact.

[1] Supported by grants from the Medical Research Council of the United Kingdom, Cancer Research United Kingdom Grants C153/A1797 and/A1802, and an educational grant from Schering-Plough Ltd.

[2] To whom requests for reprints should be addressed, at Molecular Imaging Centre, Academic Department of Radiation Oncology, Christie NHS Trust Hospital, Wilmslow Road, Manchester M20 4BX, United Kingdom. Phone: 44-161-446-8003; Fax: 44-161-446-8111; E-mail: Anne.Mason@christie-tr.nwest.nhs.uk.

[3] The abbreviations used are: DTIC, dacarbazine; MTIC, 5-(3-methyltriazen-1-yl)imidazole-4-carboxamide; PET, positron emission tomography; TAC, time-*versus*-radioactivity curve; $AUC_{p(0-90\ min)}$, area under the plasma time-*versus*-radioactivity curve between 0 and 90 min; IRF, impulse response function.

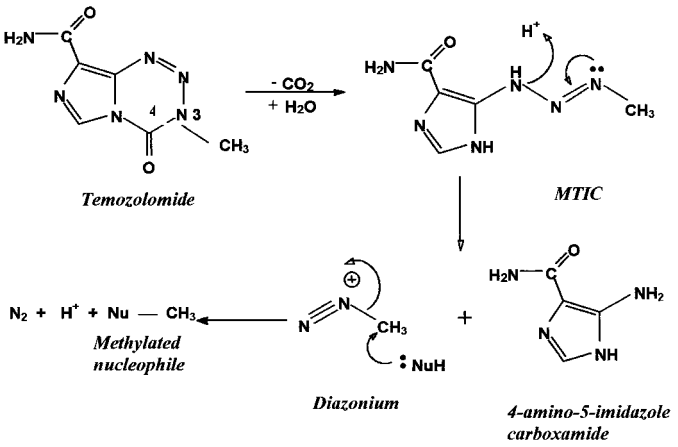

Fig. 1. Mechanism of action of temozolomide. It was postulated that radiolabel in the 3-*N*-methyl position of temozolomide would be retained ultimately by the alkylating species after ring opening of temozolomide. On the other hand the radiolabel in the 4-carbonyl position will get converted to [^{11}C]carbon dioxide, which can be detected in the exhaled air and plasma.

plasma and tissue [^{11}C]CO_2. Therefore, it was possible to deduce tissue pharmacokinetics of [^{11}C]temozolomide with both [3-*N*-^{11}C-methyl]temozolomide and [4-^{11}C-carbonyl]temozolomide. Furthermore, we proposed that if the postulated mechanism of chemical breakdown were confirmed, then the proportion of radiolabeled temozolomide out of the total radiotracer in tissue with [4-^{11}C-carbonyl]temozolomide administration would give an indication of the amount of chemical conversion of [^{11}C]temozolomide.

MATERIALS AND METHODS

Patients. Six patients (all male; 27–63 years of age) were studied. All had histologically proven gliomas and a WHO performance status of 0, 1, or 2. Mentally unstable patients and those who had previous radiotherapy within the last 4 weeks were excluded from the study. Patients gave written informed consent to take part in the study, which had approval from the Hammersmith Hospital Research Ethics Committee and the Administration of Radioactive Substances Advisory Committee, United Kingdom.

Study Design and Procedure. Each patient underwent two PET studies (A and B) after the injection of ^{11}C (half-life 20.1 min) -radiolabeled temozolomide with a period of at least a week in between the study periods. In study period A, two PET scans were performed, one after an infusion of ^{15}O (half-life 2.1 min) -labeled water to define vasculature and to aid in the definition of regions of interest (10 min duration) and another scan (90 min) after the injection of [3-*N*-^{11}C-methyl]temozolomide. Period B also consisted of two PET scans, a PET scan after injection of [^{11}C]HCO_3 (60 min) to correct for the contribution of [^{11}C]CO_2 and another scan after the injection of [4-^{11}C-carbonyl]temozolomide (90 min). The initial PET scan was performed in one of the two study periods followed by the other. Radiolabelled temozolomide and bicarbonate were injected as bolus injections over ~30 s, whereas radiolabeled water was given over 20 s.

All of the scans were conducted as an outpatient procedure at the MRC Cyclotron Unit at the Hammersmith Hospital. Before each scan an arterial cannula was inserted into the radial artery under local anesthesia for plasma sampling throughout the scan. A venous line was also inserted for administration of the radiotracers. Patients were positioned on the scanner using laser beams for alignment. PET scanning was performed on an ECAT 953 (three-dimension) scanner (CTI/Siemens, Knoxville, TN; Ref. 9). This scanner allows simultaneous data acquisition to form 31 *trans*-axial planes with axial field of view of 10.8 cm (average full width at half-maximum = 5.8 mm). To enable correction for attenuation of photons in the body, a transmission scan was performed using a rotating ^{68}Ge/^{68}Ga rod source before tracer injection.

Radiochemical Synthesis. [3-*N*-^{11}C-methyl]temozolomide was synthesized as reported previously (10, 11). Briefly, [^{11}C-methyl]methylisocyanate was synthesized by passing [^{11}C]iodomethane in nitrogen over silver cyanate. Reaction of [^{11}C-methyl]methylisocyanate with the diazo precursor (5-diazoimidazole-4-carboxamide) yielded [3-*N*-^{11}C-methyl]temozolomide. For the synthesis of [4-^{11}C-carbonyl]temozolomide, [^{11}C-carbonyl]methyl isocyanate was prepared from [^{11}C]phosgene. Reaction of [^{11}C-carbonyl]methyl isocyanate with the diazo precursor resulted in the production of [4-^{11}C-carbonyl]-temozolomide. [^{11}C]bicarbonate was prepared as [^{11}C]sodium bicarbonate by the reaction of aqueous sodium hydroxide with [^{11}C]carbon dioxide.

Tracer quantities of temozolomide (mean, 1.35 μg; range, 0.47–2.59 μg) were administered during each of the scans and were at least 1/50,000 of the therapeutic dose range (150–200 mg/m^2/day). The mean injected radioactivity of [3-*N*-^{11}C-methyl]temozolomide and [4-^{11}C-carbonyl]temozolomide was 258 MBq (range, 181–352) and 172 MBq (range, 114–269), respectively. These were associated with mean specific activities of 28.4 GBq (range, 17.7–37.4) and 40.1 GBq (range, 24.4–73.0), for [3-*N*-^{11}C-methyl]temozolomide and [4-^{11}C-carbonyl]temozolomide, respectively. Mean radiochemical purity of the injected [^{11}C]temozolomide was 97.8% (range, 90.6–100). Similarly, the mean activity of [^{11}C]bicarbonate was 369 MBq (range, 351–378), with a radiochemical purity of 100%.

Plasma Sampling. Plasma sampling was performed simultaneously with PET data acquisition throughout the PET study, to enable comparison of tissue radioactivity with plasma input. Continuous sampling of arterial blood radioactivity concentrations was performed via the arterial cannula. In addition, discrete plasma samples were also obtained at 2.5, 5, 10, 20, 40, 60, 75, and 90 min to ascertain the contribution of parent [^{11}C]temozolomide and ^{11}C-labeled metabolites to total plasma radioactivity.

Besides plasma [^{11}C]temozolomide radioactivity, the contribution of [^{11}C]CO_2 and other [^{11}C]metabolites to blood radioactivity was also determined. Metabolite analysis of [^{11}C]CO_2 was performed as described previously (12). Briefly, an aliquot of blood was mixed in sodium hydroxide, which trapped all of the [^{11}C]activity, including all of the [^{11}C]CO_2 (C_{total}), as soon as the sample was withdrawn. Isopropanol and hydrochloric acid were added to another aliquot of blood, sample mixed, and nitrogen bubbled through it to release the [^{11}C]CO_2. The activity remaining after the removal of [^{11}C]CO_2 is given as C_{rem}. From this the percentage of [^{11}C]CO_2 (C_{CO2}) was given as:

$$C_{CO2} = \frac{C_{total} - C_{rem}}{C_{total}} \times 100$$

A third aliquot of blood was taken from the same sample of blood for analysis of [^{11}C]temozolomide and other [^{11}C]metabolites. This was centrifuged to obtain plasma, which was acidified to prevent chemical decomposition of [^{11}C]temozolomide. The plasma sample was deproteinized by addition of ice-cold acetonitrile, centrifuged, and the supernatant concentrated by rotary evaporation. The residue was dissolved in high-performance liquid chromatography mobile phase, filtered, and the filtrate analyzed on a reverse-phase column C18 μ-Bondapak column (300 × 7.8 mm; 10 μm) using a mobile phase of ammonium acetate (50 mM) and acetonitrile [95:5 v/v (pH 6.7)] at 3 ml/min. The eluate was monitored with UV absorbance at 323 nm and radioactivity. If the percentage of [^{11}C]temozolomide out of total activity in this sample was Ctmz, then the percentage of [^{11}C]temozolomide in plasma (Cpltmz) was given as:

$$C_{pltem} = (100 - C_{CO2}) \times C_{tmz}$$

Plasma Pharmacokinetics. Plasma radioactivity was initially corrected for physical decay, and [^{11}C]temozolomide radioactivity (kBq/ml) was derived from the fraction of [^{11}C]temozolomide in plasma at various time points. TACs for [^{11}C]temozolomide were generated and the $AUC_{p(0-90\ min)}$ was calculated using the trapezoidal method. Systemic clearance between 0 and 90 min (Cl_{0-90}) was estimated from the injected dose of [^{11}C]temozolomide (kBq) and the $AUC_{p(0-90\ min)}$ (Dose/$AUC_{p(0-90\ min)}$).

PET Data Analysis. Sinograms were corrected for attenuation, detector efficiency (scatter, randoms, and dead-time), and detector nonuniformity, and reconstructed into tomographic images using the standard filtered back-projection algorithm (13). PET image data were calibrated to kBq/ml. Regions of interest on normal brain (gray and white matter) and tumor were manually defined on the PET images, with the aid of ^{15}O PET scans and/or computed tomography/magnetic resonance imaging films using the image-analysis soft-

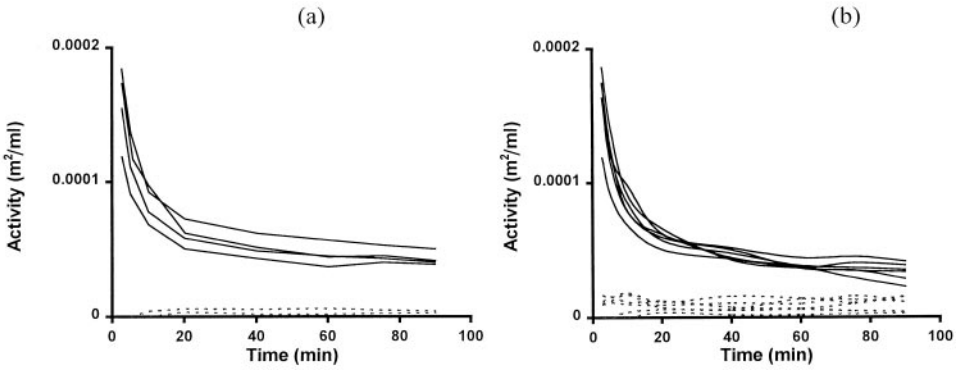

Fig. 2. Plasma TACs for [^{11}C]temozolomide (*unbroken lines*) after injection of [3-*N*-^{11}C-methyl]temozolomide (*a*) and [4-^{11}C-carbonyl]temozolomide (*b*). [^{11}C]CO_2 (*broken lines*) was identified in all patients after [4-^{11}C-carbonyl]temozolomide administration but was identified in only two of the four studies after [3-*N*-^{11}C-methyl]temozolomide.

ware, Analyze (Mayo Clinic, Rochester, MN). The radioactivity per unit volume for each region of interest was derived for each time frame to obtain TACs. TACs were corrected for the physical decay of radioactivity and normalized to injected dose per body surface area. The AUC for each tissue was calculated from 0 to 90 min ($AUC_{0-90\ min}$) as described previously (14) to give a measure of overall tissue/tumor tracer exposure.

Correction for Tissue Metabolites. As PET tissue data are unable to distinguish between the radiolabeled chemical forms of a compound *in vivo*, a data-led analytical approach (15) was adopted to quantify the contribution of metabolites in the tissue data. Because it was envisaged that [^{11}C]CO_2 would be the primary metabolite in this study, an additional scan was performed after injection of [^{11}C]HCO_3 to account for the contribution of [^{11}C]CO_2 to the tissue image. The rapid conversion and equilibration of [^{11}C]HCO_3 to [^{11}C]CO_2 by the action of carbonic anhydrase in plasma was the basis for using [^{11}C]HCO_3 to account for the contribution of [^{11}C]CO_2. A similar correction for the contribution of [^{11}C]CO_2 to the tissue data has been validated previously by our group in the evaluation of [^{11}C]thymidine PET scans, where the principal metabolite is also [^{11}C]CO_2 (16).

The contribution of [^{11}C]CO_2 to the tissue data was corrected using spectral analysis (15), a general deconvolution technique applied previously in oncology studies (16–18). Briefly, the relationship between plasma and tissue [^{11}C]CO_2 in the [^{11}C]HCO_3 scan was derived and referred to as unit IRF.

$$\text{Tissue } [^{11}\text{C}]CO_2(t) = \text{IRF}(t) \otimes \text{Plasma } [^{11}\text{C}]CO_2(t) \text{ (Bicarbonate scan)}$$

This relationship [IRF(t)] between plasma and tissue [^{11}C]CO_2 was used to derive the tissue contribution of [^{11}C]CO_2, in the temozolomide scans:

$$\text{Plasma } [^{11}\text{C}]CO_2 \otimes \text{IRF}(t) = \text{Tissue } [^{11}\text{C}]CO_2(t) \text{ (Temozolomide scan)}$$

From this the contribution of [^{11}C] temozolomide to the tissue image was derived as follows:

$$\text{Tissue } [^{11}\text{C}]\text{temozolomide}(t) = \text{Tissue } [^{11}\text{C}]\text{total}(t) - \text{Tissue } [^{11}\text{C}]CO_2(t)$$

Derivation of Ring Opening over 90 Min. If the hypothetical mechanism of chemical breakdown of temozolomide was true, then the generation of [^{11}C]CO_2 after administration of [4-^{11}C-carbonyl]temozolomide would be indicative of the ring opening of [^{11}C]temozolomide, and the amount of [^{11}C]CO_2 generated would enable quantification of the total ring opening in the body for the scan duration (90 min). Therefore, ring opening over 90 min was derived after administration of [4-^{11}C-carbonyl]temozolomide from the ratio of total [^{11}C]temozolomide activity to the total [^{11}C]tracer activity and expressed as percentage ring opening ($\times$100%),

$$\text{Ring opening over 90 min} = 1 - \frac{AUC_{0-90}[^{11}\text{C}]\text{temozolomide}}{AUC_{0-90}[^{11}\text{C}]\text{total tracer}}$$

Thus, if there was no ring opening, then all of the activity over 90 min in the [4-^{11}C-carbonyl]temozolomide scan would be from [^{11}C]temozolomide. Using this method, ring opening over 90 min was calculated in plasma, normal tissue, and tumor. This method assumes that breakdown of temozolomide occurs only by ring opening at the 3–4 position, with decarboxylation resulting in the generation of [^{11}C]CO_2 from the radiolabeled carbon atom in the C-4 position.

Sampling of Exhaled Air. Exhaled [^{11}C]CO_2 was sampled for the full duration of the scan by a loose-fitting single-use nasal oxygen set (Portex, Hythe, United Kingdom), the stems of which were positioned in the nostrils of the patient, as described previously (19). Air was drawn from the nasal set through a plastic scintillation detector to which it was connected using a nonpulsatile air pump set at 1.5 liter/min. The scintillation counter was cross-calibrated against a high-pressure ion chamber for purposes of quality control and assurance. The air line was also sampled downstream of the detector through a capnograph at a rate of 0.25 liter/min. Patients were asked to breathe normally through their nose during the procedure.

Exhaled [^{11}C]CO_2 that was sampled for the full scan duration was corrected for physical decay and normalized for the injected activity of the radiotracer. This allowed the determination of exhaled [^{11}C]CO_2 per ml of exhaled air, and the TACs of exhaled [^{11}C]CO_2 were plotted. For ease of comparison, the [^{11}C]CO_2 activities were calculated and expressed in units of % injected dose/ml of exhaled air. From this the total amount of exhaled [^{11}C]CO_2 in each ml of sampled air over 90 min was calculated for both labels of temozolomide and compared.

No attempt was made to collect all of the exhaled air, as this would be associated with considerable patient discomfort and logistical difficulties in the conduct of PET scanning.

Statistical Methods. Paired and unpaired plasma and tissue data were compared by Wilcoxon and Mann-Whitney *t* tests, respectively. Summary statistics and statistical comparisons were generated using STATA version 5.0 (Stata Corporation, College Station, TX). *P*s $\leq$ 0.05 were considered significant.

RESULTS

All of the patients completed both scanning periods except subject 3, whose condition deteriorated before the second set of scans (period A). PET images for patient 1 were lost because of technical problems during the first set of scans (period A). However, plasma and exhalation data were available for analyses. Thus, 6 PET images were available for analyses from period B and 4 from period A.

Plasma Pharmacokinetics. After administration of [^{11}C]temozolomide, [^{11}C]CO_2 was identified in addition to [^{11}C]temozolomide in plasma. Plasma [^{11}C]CO_2 was detected for all of the studies after injection of [4-^{11}C-carbonyl] temozolomide (Fig. 2*b*), and in two of the four studies after administration of [3-*N*-^{11}C-methyl]temozolomide (Fig. 2*a*). No other ^{11}C-labeled metabolites of [^{11}C]temozolomide were identified for both labeling positions. The contribution of [^{11}C]temozolomide to total plasma radioactivity was higher when temozolomide was radiolabelled in the 3-*N*-methyl position. The mean (SE) percentage of contributions of [^{11}C]temozolomide, [^{11}C]CO_2, and unidentified [^{11}C]metabolites to the total [^{11}C] plasma radioactivity at 10 min with [3-*N*-^{11}C-methyl]temozolomide were 92.88 (3.9), 1.23 (1.2), and 5.90 (2.8), respectively. In comparison, mean (SE) percentage contributions of [^{11}C]temozolomide, [^{11}C]CO_2, and unidentified ^{11}C metabolites to the total ^{11}C plasma radioactivity at 10 min with [4-^{11}C-carbonyl]temozolomide were 85.75 (2.1), 12.3

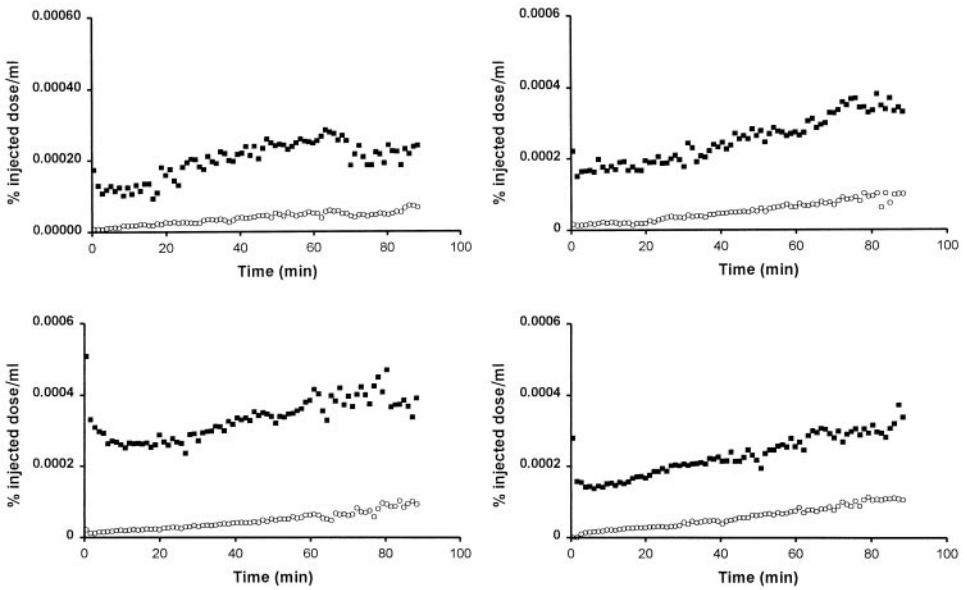

Fig. 3. TACs of exhaled $[^{11}C]CO_2$ for four patients after injection of $[^{11}C]$temozolomide. The *top plots* (■) in each of the graphs are after injection of [4-^{11}C-carbonyl]temozolomide and the *bottom plots* (○) after administration of [3-*N*-^{11}C-methyl]temozolomide.

(1.9), and 1.96 (0.9), respectively. Similarly, at 90 min the mean (SE) percentage of contributions of $[^{11}C]$temozolomide, $[^{11}C]CO_2$, and unidentified ^{11}C metabolites to total plasma radioactivity were 91.97 (0.7), 4.16 (2.5), and 3.87 (2.2) with [3-*N*-^{11}C-methyl]temozolomide, and 65.68 (4.6), 27.72 (2.0), and 6.6 (5.3) with [4-^{11}C-carbonyl]temozolomide, respectively. It was noted that $[^{11}C]CO_2$ was still generated (albeit in small quantities) with [3-*N*-^{11}C-methyl]temozolomide.

Cl_{0-90} of $[^{11}C]$temozolomide was unaffected by the position of the radiolabel on the temozolomide molecule ($P > 0.05$) with mean (SE) Cl_{0-90} being 0.195 (0.01) liters/min/m^2 and 0.212 (0.01) liters/min/m^2 with [3-*N*-^{11}C-methyl]temozolomide and [4-^{11}C-carbonyl]temozolomide, respectively. The similar clearance values of both radiolabeled forms would suggest the lack of any inherent instability in either of the two radiolabeled molecules. Plasma pharmacokinetic parameters were not estimated to infinity, as >25% extrapolation from C_{last} was obtained in some instances.

Exhaled $[^{11}C]CO_2$. As with plasma data, $[^{11}C]CO_2$ was detected in exhaled air after the injection of both radiolabeled forms of temozolomide (Fig. 3). However, a larger proportion ($P < 0.05$) was detected after injection of [4-^{11}C-carbonyl]temozolomide. The total amount of exhaled $[^{11}C]CO_2$ per ml of exhaled air with [4-^{11}C-carbonyl] temozolomide [mean (SE)] was 1.18 (0.09) % of injected dose. In contrast, the amount of exhaled $[^{11}C]CO_2$ in each ml of exhaled air with [3-*N*-^{11}C-methyl]temozolomide was [mean (SE)] 5-fold lesser at 0.23 (0.02) % of injected dose ($P < 0.05$).

Normal Tissue and Tumor Kinetics. Visual inspection of PET images revealed that there was uptake of radiotracer (^{11}C-labeled temozolomide and metabolites) in both normal tissue and tumor (Fig. 4). To determine whether there was any difference in radiotracer exposure between the two labels, the radiotracer $AUC_{0-90\ min}$ was calculated for normal tissue and tumor (Table 1). There was no difference in radiotracer exposure between both radiolabeled forms of temozolomide for the individual tissues. The similar AUC values noted with both forms would indicate that the parent compound (temozolomide) and its metabolites have similar properties of uptake by the tissues. Of potential therapeutic importance was the greater radiotracer exposure in tumors compared with normal tissue with both radiotracers. This may be because of either specific tumor targeting by temozolomide and its metabolites or may just reflect an impaired blood-brain barrier in patients with brain tumors.

Spectral analytical methodology was used to correct for the contribution of $[^{11}C]CO_2$ (the major and only radiolabelled molecule identified) to the tissue images (15, 16). This is illustrated in Fig. 5. Fig. 5, *a* and *b*, illustrate the TAC in tumor and gray matter, respectively, for a subject after injection of [3-*N*-^{11}C-methyl]temozolomide. As $[^{11}C]CO_2$ was not identified in plasma, in this study, no corrections were made for metabolites. Therefore, the total radiotracer activity in this instance is indicative of tissue $[^{11}C]$temozolomide activity. Fig. 5, *c* and *d*, illustrate TACs in tumor and gray matter, respectively, in the same subject after injection of [4-^{11}C-carbonyl]temozolomide, where plasma $[^{11}C]CO_2$ contribution was substantial. The top plots in Fig. 5 (unbroken lines) represent the total tracer (^{11}C-labeled parent and metabolites) activity. From this the contribution of $[^{11}C]CO_2$ to the total tracer activity was deconvolved using spectral analysis. This contribution of $[^{11}C]CO_2$ to tissue activity is plotted as a $[^{11}C]CO_2$ TAC (Fig. 5, closed triangles). The contribution of $[^{11}C]$temozolomide was obtained by subtracting $[^{11}C]CO_2$ activity from the total

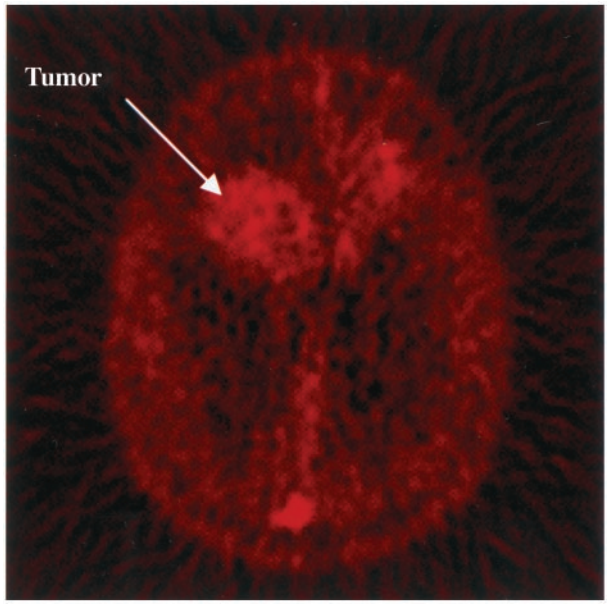

Fig. 4. PET image showing uptake of [3-*N*-^{11}C-methyl]temozolomide by tumor and normal brain.

Table 1 *Comparison of total [^{11}C] tracer and [^{11}C] CO_2-corrected [^{11}C] temozolomide exposure ($AUC_{0-90\ min}$) after injection of [3-*N*-^{11}C-methyl] temozolomide and [4-^{11}C-carbonyl] temozolomide*

Comparison between tissues demonstrated total [^{11}C]tracer exposure in tumors was higher in tumor compared with normal tissue ($P < 0.05$). Similarly, [^{11}C]temozolomide exposure was higher in tumors compared with normal tissue, reaching significance ($P < 0.05$) with [4-^{11}C-carbonyl]temozolomide studies ($n = 6$), but not with [3-*N*-^{11}C-methyl]temozolomide ($n = 4$). Comparison within tissues showed no differences in exposure to total tracer when temozolomide was injected labeled in either of the positions. In contrast, exposure to [^{11}C]temozolomide was higher within tissues after [3-*N*-^{11}C-methyl]-temozolomide injections tending towards significant levels ($P = 0.07$ for all tissues).

	Total [^{11}C]tracer $AUC_{0-90\ min}$ Mean (SE) m^2/ml		[^{11}C]temozolomide $AUC_{0-90\ min}$ Mean (SE) m^2/ml	
	[3-*N*-^{11}C-methyl] temozolomide	[4-^{11}C-carbonyl] temozolomide	[3-*N*-^{11}C-methyl] temozolomide	[4-^{11}C-carbonyl] temozolomide
Tumor	0.134 (0.03)	0.136 (0.01)	0.128 (0.03)	0.101 (0.01)
Grey matter	0.107 (0.005)	0.110 (0.001)	0.102 (0.008)	0.077 (0.002)
White matter	0.074 (0.007)	0.081 (0.004)	0.070 (0.005)	0.056 (0.004)

tracer activity at the mid-frame times of the PET scans. This corrected [^{11}C]temozolomide TAC is plotted in Fig. 5 as closed squares. The contribution of the other unidentified [^{11}C]metabolites was not modeled in both the groups of PET images (*i.e.,* [^{11}C]temozolomide and non-[^{11}C]CO_2 metabolites were grouped together).

Tissue exposure (AUC_{0-90}) to [^{11}C]temozolomide was compared between the two sets of scans (Table 1). Similar to total tracer $AUC_{0-90\ min}$, [^{11}C]temozolomide exposure ($AUC_{0-90\ min}$) was greater in tumor compared with normal tissue and was statistically significant in studies performed after injection of [4-^{11}C-carbonyl] temozolomide ($P < 0.05$; $n = 6$), but not after injection of [3-*N*-^{11}C-methyl] temozolomide ($P > 0.05$; $n = 4$). Comparison was also made between [^{11}C]temozolomide tissue exposure after injection of temozolomide labeled in either of the two positions. In contrast to total tracer exposure, [^{11}C]temozolomide $AUC_{0-90\ min}$ was higher in all of the tissues when it was labeled in the 3-*N*-methyl position, although this did not reach statistical significance ($P = 0.07$ in tumor, gray, and white matter).

Percentage Ring Opening. Ring opening of [^{11}C]temozolomide over 90 min was calculated in plasma, normal tissue, and tumor (Table 2). The percentage ring opening in plasma over 90 min (20.89%) was less ($P < 0.05$) than that observed in tumor (26.78%), gray matter (29.70%), and white matter (30.13%). However, there were no differences in the amount of observed ring opening between tumor and normal tissues ($P > 0.05$).

DISCUSSION

Temozolomide is an alkylating agent that is structurally related to DTIC, with both drugs requiring conversion to the cytotoxic intermediate MTIC for clinical activity. Preclinical and mechanistic studies predicted a potential clinical advantage for temozolomide based on the nonenzymatic, pH-dependent generation of MTIC, which optimally occurs at physiological pH (6, 20, 21). This potential therapeutic advantage has been confirmed by clinical studies that have demonstrated promising anticancer activity particularly in patients with central nervous system malignancies and melanoma (22, 23). In addition, low interpatient variability in temozolomide clearance and excellent oral bioavailability (3) indicate a significant therapeutic advantage for temozolomide over i.v. DTIC, which requires metabolic activation via cytochrome P450 enzymes. Although MTIC was originally proposed as the alkylating species, it is now understood that the highly reactive methanediazonium ion produced by the reaction of MTIC with water at physiological pH is responsible for the methylating effect of temozolomide (6).

The site at which the conversion of temozolomide to MTIC occurs has been the subject of much speculation. It was initially proposed that conversion occurs in the DNA, with runs of guanine residues representing an accessible nucleophilic and basic microenvironment, which would facilitate conversion of temozolomide to MTIC, possibly by an "activated" water molecule in the major groove of the DNA. The electronic and steric effects of runs of three or more guanines were thought to enhance the nucleophilicity resulting especially in the methylation of the middle guanine of the N-7 residue (6). This theory was supported by the observation that MTIC preferentially methylates the N-7 residue (24). Against this theory was the observation that temozolomide activity correlated with the O^6 methylation, with tumor cell lines expressing high levels of O^6-alkyl-DNA alkyltransferase repair protein being refractory to temozolomide treatment (25, 26). In

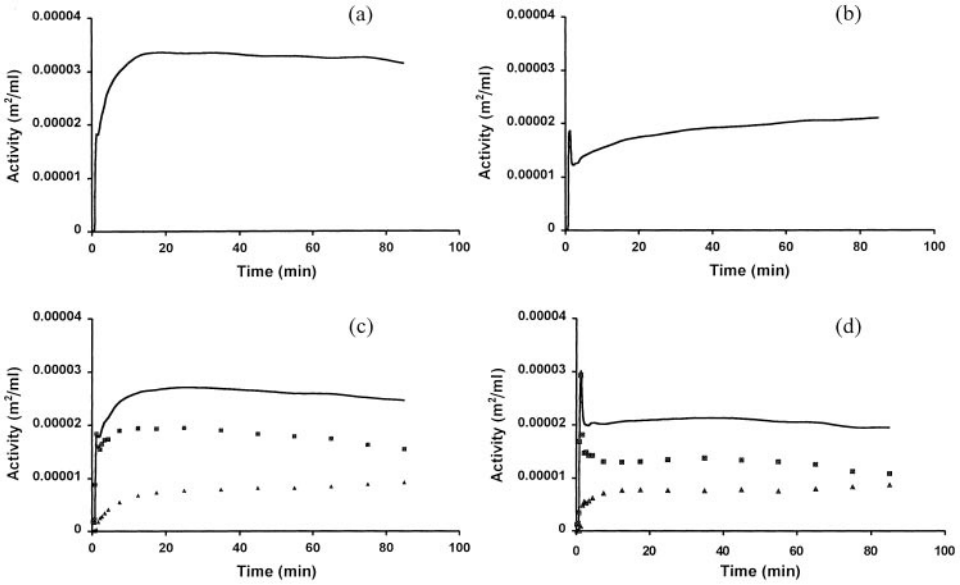

Fig. 5. Tissue TACs for tumor (*a* and *c*) and gray matter (*b* and *d*) after injection of [^{11}C]temozolomide. Plots *a* and *b* are after injection of [3-*N*-^{11}C-methyl]temozolomide, and plots *c* and *d* after injection of [4-^{11}C-carbonyl]temozolomide. As plasma [^{11}C]CO_2 was not detected after [3-*N*-^{11}C-methyl]temozolomide in this patient, total tracer TAC was not corrected for metabolites. TACs were corrected for the contribution of [^{11}C]CO_2 after administration of [4-^{11}C-carbonyl]temozolomide. Plots *c* and *d* represent the total tissue tracer TAC (*unbroken line*), tissue [^{11}C]temozolomide TAC (■) and tissue [^{11}C]CO_2 TAC (▲). Metabolite correction was performed using spectral analysis.

Table 2 *Percentage ring opening of [^{11}C]temozolomide for the full duration of the scan*

This was calculated from the ratio of total [^{11}C]tracer: [^{11}C]temozolomide after injection of [4-^{11}C-carbonyl] temozolomide. Ring opening was greater in tissues compared with plasma ($P < 0.05$). However, there was no tumor-specific ring opening, as no differences in percentage ring opening were observed between tumor and normal tissues.

Patient no.	Plasma	Tumor	Grey matter	White matter
1	18.73	26.89	28.32	26.80
2	27.79	33.33	26.13	26.56
3	21.54	20.58	27.78	28.75
4	21.04	30.66	38.18	38.36
5	18.99	21.78	29.36	28.24
6	17.25	27.42	28.44	32.05
Mean	20.89	26.78	29.70	30.13
(SE)	(1.5)	(2.0)	(1.8)	(1.8)

addition, all of the alkylating agents were associated with N-7 methylation, which was a characteristic of DNA rather than cytotoxic agents. Proof against DNA-based conversion of temozolomide was additionally supported from molecular modeling studies, which showed that the conversion of temozolomide occurs in free solution under the influence of local pH and additional DNA footprinting studies that were unable to detect noncovalent associations between DNA and temozolomide (5). The current thinking is that ring opening of temozolomide is entirely pH dependent and is supported by studies that have demonstrated that plasma half-life of temozolomide is in accord with the observed half-life of temozolomide in phosphate buffer (pH 7.4) at 37°C; Refs. 2, 3, 6).

In this study, we have applied PET methodology to investigate the mechanism of breakdown and, hence, the therapeutic rationale of the mechanism of action of temozolomide. Specifically, we investigated if the proposed mechanism of action of temozolomide could be demonstrated *in vivo* in man using a dual radiolabeling strategy. Our hypothesis was that if ring opening of temozolomide occurs in the 3–4 position, as proposed, then the radiolabel will be carried either by the alkylating species or by carbon dioxide, when temozolomide was radiolabelled in the 3-N-methyl or 4-carbonyl positions, respectively. We found support for this hypothesis when we sampled a 5-fold higher amount of exhaled [^{11}C]CO_2 with [4-^{11}C-carbonyl]temozolomide administration. In addition, significant concentration of plasma [^{11}C]CO_2 was detected with [4-^{11}C-carbonyl]temozolomide in contrast to small quantities of [^{11}C]CO_2 detected in plasma in two of the four studies with [3-*N*-^{11}C-methyl]temozolomide. Supporting evidence was provided by tissue data, where a decrease in tissue exposure ($AUC_{0-90\ min}$) to [^{11}C]temozolomide was observed with [4-^{11}C-carbonyl] temozolomide compared with [3-*N*-^{11}C-methyl]temozolomide, indicating the loss of radiolabel as [^{11}C]CO_2. These data provide proof of principle of the postulated metabolic breakdown of temozolomide. However, it was also observed in these studies that [^{11}C]CO_2 (albeit small quantities) was still generated when [3-*N*-^{11}C-methyl] temozolomide was administered. The source of this [^{11}C]CO_2 is unclear with the existence of an alternative metabolic pathway being a possibility, in addition to that postulated above or by processing of the methyl group via the folate pathway.

In addition to ring opening, we also evaluated the plasma and tissue pharmacokinetics of [^{11}C]temozolomide in this study. [^{11}C]temozolomide was identified as the major radiolabeled compound in plasma for both set of studies, with [^{11}C]CO_2 being the primary elimination product of [^{11}C]temozolomide. We were unable to identify any of other radiolabeled metabolites contributing to plasma radioactivity. The relatively short duration of the scan (90 min) compared with the half-life of the temozolomide (114 min; Ref. 3) limited the plasma pharmacokinetic parameters that could be calculated; the pharmacokinetic parameters calculated in such instances from PET studies predominantly reflect distribution and initial elimination of the drug. The calculated clearance between 0 and 90 min of [^{11}C]temozolomide was 0.2 liter/min/m^2 was higher than that estimated with other clinical studies (0.1 liter/min/m^2) and was in keeping with the shorter duration of plasma sampled with this study.

In tissues, equivalent uptake of the radiotracer was demonstrated in both normal tissues and tumor with both forms of temozolomide, implying the absence of any molecular entities, which were sequestrated in the plasma. Of interest and of potential therapeutic value in the clinical efficacy of temozolomide was the higher tumor exposure ($AUC_{0-90\ min}$) seen with temozolomide and total radiotracer compared with surrounding normal tissue. The higher $AUC_{0-90\ min}$ observed for [^{11}C]temozolomide in tumors compared with white and gray matter may provide a beneficial therapeutic index that may account for the clinical efficacy of temozolomide seen in gliomas (23). It is worth noting that the higher $AUC_{0-90\ min}$ seen in brain tumors compared with normal brain may be related to a compromised blood-brain barrier and, hence, higher delivery, rather than retention of temozolomide. In this method, the contribution of non-[^{11}C]CO_2 metabolites (plasma contribution of non-[^{11}C]CO_2 metabolites was similar with both radiolabelled forms) to tissue radioactivity was not modeled separately.

Having confirmed the mechanism of breakdown of temozolomide, we set out to answer whether there was a differential in ring opening among plasma, normal tissue, and tumor, which may represent a targeted method of drug action in the tumor. If such a differential existed this would lend some support to the original hypothesis on temozolomide metabolism, where it was proposed that metabolic conversion occurred in DNA (6). In this study, we found a higher percentage of ring opening at 90 min in tissues compared with plasma, indicative of targeted tissue action as opposed to plasma. However, there was no difference in ring opening between tumors and normal tissue, suggesting that ring opening of temozolomide was tissue-specific but not tumor-specific. The methodology used to determine ring opening in tissues has a potential drawback in that it reflects both tissue-specific decarboxylation and influx of [^{11}C]temozolomide and [^{11}C]CO_2 from the blood stream. Nevertheless, the inference on the differential in ring opening between plasma and tissue may still be true (although to a varying degree), as a higher amount of ring opening was observed in tissue despite the contribution from plasma, wherein ring opening was less. As a concluding remark of caution, we would like to state that calculation of the tissue metabolite correction is dependent on the method of analysis, which in the past has proven to be robust (16).

In conclusion, we have used PET methodology to ascertain the *in vivo* mechanism of metabolic breakdown of temozolomide using tracer amounts of the drug. In addition, this study has provided important information on tumor and normal tissue pharmacokinetics, not available by other means.

REFERENCES

1. Stevens, M. F., Hickman, J. A., Stone, R., Gibson, N. W., Baig, G. U., Lunt, E., and Newton, C. G. Antitumor imidazotetrazines. 1. Synthesis and chemistry of 8-carbamoyl-3-(2-chloroethyl)imidazo[5, 1-d]-1, 2, 3, 5-tetrazin-4(3 H)-one, a novel broad-spectrum antitumor agent. J. Med. Chem., *27:* 196–201, 1984.
2. Newlands, E. S., Blackledge, G. R., Slack, J. A., Rustin, G. J., Smith, D. B., Stuart, N. S., Quarterman, C. P., Hoffman, R., Stevens, M. F., Brampton, M. H., and Gibson, A. C. Phase I trial of temozolomide (CCRG 81045: M&B 39831: NSC 362856). Br. J. Cancer, *65:* 287–291, 1992.
3. Baker, S. D., Wirth, M., Statkevich, P., Reidenberg, P., Alton, K., Sartorius, S. E., Dugan, M., Cutler, D., Batra, V., Grochow, L. B., Donehower, R. C., and Rowinsky, E. K. Absorption, metabolism, and excretion of 14C-temozolomide following oral administration to patients with advanced cancer. Clin. Cancer Res., *5:* 309–317, 1999.
4. Newlands, E. S., Stevens, M. F., Wedge, S. R., Wheelhouse, R. T., and Brock, C. Temozolomide: a review of its discovery, chemical properties, pre- clinical development and clinical trials. Cancer Treat. Rev., *23:* 35–61, 1997.

5. Clark, A. S., Deans, B., Stevens, M. F. G., Tisdale, M. J., Wheelhouse, R. T., Denny, B. J., and Hartley, J. A. Antitumor imidazotetrazines. 32. Synthesis of novel imidazotetrazinones and related bicyclic heterocycles to probe the mode of action of the antitumor drug temozolomide. J. Med. Chem., *38:* 1493–504, 1995.
6. Denny, B. J., Wheelhouse, R. T., Stevens, M. F., Tsang, L. L., and Slack, J. A. NMR and molecular modeling investigation of the mechanism of activation of the antitumor drug temozolomide and its interaction with DNA. Biochemistry, *33:* 9045–9051, 1994.
7. Saleem, A., Yap, J., Osman, S., Brady, F., Suttle, B., Lucus, S. V., Jones, T., Price, P. M., and Aboagye, E. O. Modulation of fluorouracil tissue pharmacokinetics by eniluracil: *in-vivo* imaging of drug action. Lancet, *355:* 2125–2131, 2000.
8. Saleem, A., Harte, R. J., Matthews, J. C., Osman, S., Brady, F., Luthra, S. K., Brown, G. D., Bleehen, N., Connors, T., Jones, T., Price, P. M., and Aboagye, E. O. Pharmacokinetic evaluation of N-[2-(dimethylamino)ethyl]acridine-4-carboxamide in patients by positron emission tomography. J. Clin. Oncol., *19:* 1421–1429, 2001.
9. Spinks, T. J., Jones, T., Bailey, D. L., Townsend, D. W., Grootoonk, S., Bloomfield, P. M., Gilardi, M. C., Casey, M. E., Sipe, B., and Reed, J. Physical performance of a positron tomograph for brain imaging with retractable septa. Phys. Med. Biol., *37:* 1637–1655, 1992.
10. Brown, G. D., Turton, D. R., Luthra, S. K., Price, P., Jones, T., Stevens, M. F. G., Baghurst, D. R., Mingos, D. M. P., Osman, S., Water, S. L., and Brady, F. Synthesis of [11C -methyl]methylisocyanate and application of microwave heating to labelling the novel anticancer agent Temozolomide. J. Label Cmpd. Radiopharm., *35:* 100–103, 1994.
11. Brown, G. D., Brady, F., Luthra, S. K., Prenant, C., Stevens, M. F. G., Sergis, A., and Price, P. An improved radiosynthesis of 4-[11C-carbonyl]temozolomide using [11C carbonyl]methylisocyanate. J. Label Cmpd. Radiopharm., *40:* 371, 1997.
12. Shields, A. F., Graham, M. M., Kozawa, S. M., Kozell, L. B., Link, J. M., Swenson, E. R., Spence, A. M., Bassingthwaighte, J. B., and Krohn, K. A. Contribution of labeled carbon dioxide to PET imaging of carbon-11-labeled compounds. J. Nucl. Med., *33:* 581–584, 1992.
13. Brooks, R. A., and Di Chiro, G. Theory of image reconstruction in computed tomography. Radiology, *117:* 561–572, 1975.
14. Harte, R. J., Matthews, J. C., O'Reilly, S. M., Tilsley, D. W., Osman, S., Brown, G., Luthra, S. J., Brady, F., Jones, T., and Price, P. M. Tumor, normal tissue, and plasma pharmacokinetic studies of fluorouracil biomodulation with N-phosphonacetyl-L-aspartate, folinic acid, and interferon α. J. Clin. Oncol., *17:* 1580–1588, 1999.
15. Cunningham, V. J., and Jones, T. Spectral analysis of dynamic PET studies. J. Cereb. Blood Flow Metab., *13:* 15–23, 1993.
16. Gunn, R. N., Yap, J. T., Wells, P, Osman, S., Price, P., Jones, T., and Cunningham, V. J. A general method to correct PET data for tissue metabolites using a dual-scan approach. J. Nucl. Med., *41:* 706–711, 2000.
17. Meikle, S. R., Matthews, J. C., Brock, C. S., Wells, P., Harte, R. J., Cunningham, V. J., Jones, T., and Price, P. Pharmacokinetic assessment of novel anti-cancer drugs using spectral analysis and positron emission tomography: a feasibility study. Cancer Chemother. Pharmacol., *42:* 183–193, 1998.
18. Aboagye, E. O., Saleem, A., Cunningham, V. J., Osman, S., and Price, P. M. Extraction of 5-fluorouracil by tumor and liver: a noninvasive positron emission tomography study of patients with gastrointestinal cancer. Cancer Res., *61:* 4937–4941, 2001.
19. Gunn, R. N., Ranicar, A., Yap, T. J., Wells, P., Osman, S., Jones, T., and Cunningham, V. J. On-line measurement of exhaled [11C]CO2 during PET. J. Nucl. Med., *41:* 605–611, 2000.
20. Stevens, M. F., Hickman, J. A., Langdon, S. P., Chubb, D., Vickers, L., Stone, R., Baig, G., Goddard, C., Gibson, N. W., and Slack, J. A. Antitumor activity and pharmacokinetics in mice of 8-carbamoyl-3-methyl- imidazo[5, 1-d]-1, 2, 3, 5-tetrazin-4(3H)-one (CCRG 81045; M & B 39831), a novel drug with potential as an alternative to dacarbazine. Cancer Res., *47:* 5846–5852, 1987.
21. Tsang, L. L., Quarterman, C. P., Gescher, A., and Slack, J. A. Comparison of the cytotoxicity *in vitro* of temozolomide and dacarbazine, prodrugs of 3-methyl-(triazen-1-yl)imidazole-4-carboxamide. Cancer Chemother. Pharmacol., *27:* 342–346, 1991.
22. Bleehen, N. M., Newlands, E. S., Lee, S. M., Thatcher, N., Selby, P., Calvert, A. H., Rustin, G. J., Brampton, M., and Stevens, M. F. Cancer research campaign phase II trial of temozolomide in metastatic melanoma. J. Clin. Oncol., *13:* 910–913, 1995.
23. Newlands, E. S., O'Reilly, S. M., Glaser, M. G., Bower, M., Evans, H., Brock, C., Brampton, M. H., Colquhoun, I., Lewis, P., Rice-Edwards, J. M., Illingworth, R. D., and Richards, P. G. The Charing Cross Hospital experience with temozolomide in patients with gliomas. Eur. J. Cancer, *32A:* 2236–2241, 1996.
24. Hartley, J. A., Mattes, W. B., Vaughan, K., and Gibson, N. W. DNA sequence specificity of guanine N7-alkylations for a series of structurally related triazenes. Carcinogenesis (Lond.), *9:* 669–674, 1988.
25. Baer, J. C., Freeman, A. A., Newlands, E. S., Watson, A. J., Rafferty, J. A., and Margison, G. P. Depletion of O6-alkylguanine-DNA alkyltransferase correlates with potentiation of temozolomide and CCNU toxicity in human tumour cells. Br. J. Cancer, *67:* 1299–302, 1993.
26. Tisdale, M. J. Antitumor imidazotetrazines–XV. Role of guanine O6 alkylation in the mechanism of cytotoxicity of imidazotetrazinones. Biochem. Pharmacol., *36:* 457–462, 1987.

Metabolic Activation of Temozolomide Measured *in Vivo* Using Positron Emission Tomography

Azeem Saleem, Gavin D. Brown, Frank Brady, et al.

Cancer Res 2003;63:2409-2415.